

Spin Entanglement and Order Competition via Long-range Interactions in Spinor Quantum Optical Lattices

Karen Lozano-Méndez,¹ Alejandro H. Cásares,¹ and Santiago F. Caballero-Benítez^{1,*}

¹*Instituto de Física, LSCSC-LANMAC, Universidad Nacional Autónoma de México, Ciudad de México 04510, México*

Quantum matter at ultra-low temperatures offers a testbed for analysing and controlling desired properties in strongly correlated systems. Under typical conditions the nature of the atoms fixes the magnetic character the system can have. Beyond classical light potentials leading to optical lattices and short range interactions, high-Q cavities introduce novel dynamics into the system via the quantumness of light. Here we propose a theoretical model and we analyse via numerically exact simulations, the effect of cavity mediated long range magnetic interactions and optical lattices in ultracold matter. We find that global interactions allow to modify the underlying magnetic character of the system while introducing competition scenarios. Antiferromagnetic correlated bosonic matter emerges, in conditions beyond to what nature typically provides. This allows new alternatives towards the design of robust mechanisms for quantum information purposes, exploiting the properties of magnetic phases of strongly correlated quantum matter.

Magnetic quantum matter in optical lattices offers a collection of interesting phenomena in terms of quantum simulation [1]. There are possible applications ranging from the implementation of quantum computing protocols to designing properties of quantum systems. These designs could help understand underlying mechanisms that trigger different kinds of order in analog real materials. In the typical setting, the light fields act parametrically, behaving like classical waves. This allows to control them with flexibility while generating effective synthetic quantum matter solids. The degree of precision achieved allows to control the emergence of different quantum many-body phases. In this setting, strong quantum correlations are present, while paradigmatic scenarios of condensed matter systems regarding quantum phase transitions (QPT) are reproduced. Recent advances in the control of ultracold matter have allowed the experimental realisation of fermionic anti-ferromagnets [2–5]. These findings contribute to understand via quantum simulation some features linked to high-T_c superconductivity. Going beyond classical light fields by the inclusion of cavity back-action in the ultracold system, allows to control the system in new regimes. Correlations induced by the high-Q cavity light to the matter and viceversa modify significantly the energy manifolds experienced by the matter. Consequently, new correlated phases of matter can emerge. Ultracold systems without optical lattices inside high-Q cavities, but with magnetic properties, have been recently achieved by several groups [3, 7–9]. Several proposals regarding exploiting these magnetic interactions without a lattice have been put forward [10–13]. In this limit, the interplay between cavity light and internal degrees of freedom has been studied in combination with the dynamical and dissipative nature of the system. Recently, the inclusion of optical lattices and cavity back-action have been achieved [14, 15]. In these experiments, the competition of different kinds of order is possible and the optical lattice can be controlled arbitrarily. Several studies have explored possibilities linked

to this setup and QPT's [16–20]. However, the investigation of the interplay regarding magnetism in optical lattices with cavity induced interactions and strong quantum correlations remains largely unexplored.

Here we show how the interplay of magnetism, COL and cavity induced magnetic interactions allow to control of the emergence of non-trivial magnetic phases of quantum matter. As both light and matter are entangled via the cavity, effective magnetic global interactions are generated. This allows to explore quantum anti-ferromagnets efficiently. Thus, quantum state engineering of anti-ferromagnets with strong correlations can be optimised in a single setup and go beyond what the nature of the atoms typically allows.

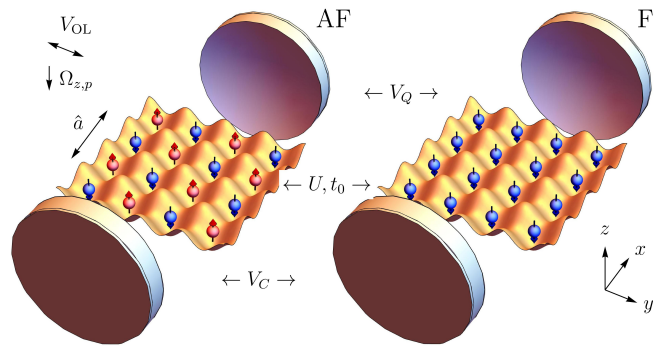


Figure 1. **Schematic of the system of ultracold atoms in a high-Q cavity with an OL and magnetic degrees of freedom.** We show typical atomic configurations with Antiferromagnetic AF (left) or ferromagnetic F (right) order. QPT's between them are possible. The optical lattice is V_{OL} with intra-cavity light \hat{a} and pumped light Rabi frequency $\Omega_{z,p}$. The effective spinor quantum optical lattice model have strengths of cavity induced magnetic interactions V_Q , intrinsic magnetic interaction V_C , on-site repulsion U and tunneling amplitude t_0 . Competing interactions and lattice depth variation change the systems between F/AF ordering.

Effective Spinor Quantum Optical Lattice model. We study ultracold bosonic atoms with $F = 1$, spin projections $\sigma \in \{\downarrow, 0, \uparrow\}$ trapped in an optical lattice (COL) subject to a constant magnetic field such that the magnetic sub-levels split. The atoms are inside a single-mode high-Q cavity with the mode frequency ω_c and decay rate κ in off-resonant scattering (see Fig.). The alkali atoms in the COL have tunneling processes with amplitude t_0 , on-site repulsion with strength U and local magnetic interactions (classical) $\propto V_C$ [2, 21]. The laser light linearly polarized is pumped into the cavity with amplitude $\Omega_{z,p}$ (in units of the Rabi frequency) and frequency ω_p ($\Delta_c = \omega_p - \omega_c$). The atoms are illuminated in a plane transverse to the cavity axis in a standing wave configuration. Each spin component of the atoms couple with cavity mode via the effective coupling strength $\tilde{g}_z = g J_z \Omega_{z,p} \sqrt{N_s} / \Delta_a$, where g is the light-matter coupling coefficient, Δ_a is the detuning between the light and atomic resonance [22]. In the COL basis (Wannier basis), the atoms are subject to the projection of the cavity light-mode with amplitude J_z over N_s sites [21]. For simplicity, we consider the COL is deep enough such that cavity-induced tunneling amplitudes (long range bond processes) are not relevant and only COL nearest neighbour tunneling processes remain (t_0) [16, 23]. Experimentally, this has been achieved in the non-magnetic version of our system [14]. The Hamiltonian of the system is $\mathcal{H} = \mathcal{H}_{\text{SCOL}} + \mathcal{H}^a + \mathcal{H}^{ab}$, where $\mathcal{H}_{\text{SCOL}} = \mathcal{H}_U + \mathcal{H}_C^S$ is the Spinor Bose-Hubbard Hamiltonian [1, 2, 21]. The light is described by $\mathcal{H}^a = -\hbar \Delta_c \hat{a}^\dagger \hat{a}$, the operators \hat{a}^\dagger (\hat{a}) create (annihilate) photons in the cavity. The light-atom magnetic interaction (\mathcal{H}^{ab}) can be controlled using the vectorial components of the polarisability encoded in $\Omega_{z,p}$ [3]. This can be generalised to the lattice case by expanding in the Wannier basis [24, 25],

$$\mathcal{H}^{ab} = \frac{\hbar}{\sqrt{N_s}} \sum_i (\tilde{g}_z \varphi_{z,i} \hat{a}^\dagger + \tilde{g}_z^* \varphi_{z,i}^* \hat{a}) \hat{S}_{z,i} \quad (1)$$

with $\hat{S}_{\nu,i} = \sum_{\xi,\xi'} \hat{b}_{\xi,i}^\dagger F_{\xi,\xi'}^\nu \hat{b}_{\xi',i}$, where $\nu \in \{x, y, z\}$ and F^ν are the angular momentum matrices for spin $S = 1$. The $\hat{b}_{\sigma,i}^\dagger$ ($\hat{b}_{\sigma,i}$) correspond to bosonic atoms at site i with spin projection σ in the COL. The function $\varphi_{z,i}$ represents the geometric factor of the overlap integrals that projects the mode structure of the light into the matter. This depends on the pump incidence angle with respect to the cavity axis and the optical lattice plane [16]. Considering the experimental situation described in [3] for the system without the optical lattice, the “ x ” and “ y ” components of the angular momentum operators are neglected due to energetics. Similar decompositions are possible in the analog Fermi system for $S = 1/2$ [26–28]. In general, the spatial structure of the light modes give a natural basis to represent collective modes depending on geometry with respect to the COL [16]. For simplicity, we have neglected the non-vectorial (non-magnetic) contributions

of the polarisability. We adiabatically eliminate light following [29]. This amounts to effectively integrating out the light in the adiabatic limit, such that $\langle \hat{a} \rangle = 0$, leading to $\langle \hat{a} \rangle \propto \sum_i \langle \tilde{g}_z \varphi_{z,i} \hat{S}_{z,i} \rangle$. We find the effective model for the Spinor Quantum Optical Lattice (SQOL),

$$\mathcal{H}_{\text{SQOL}} = \mathcal{H}_U + \frac{V_Q}{N_s} \sum_{i,j} f_{i,j}^\varphi \hat{S}_{z,i} \hat{S}_{z,j} + \frac{V_C}{2} \sum_i (\hat{\mathbf{S}}_i^2 - 2\hat{n}_i) \quad (2)$$

where $f_{i,j}^\varphi = (\varphi_{z,i}^* \varphi_{z,j} + \text{H.c.})/2$, with $V_Q = -\hbar \Delta_c |\tilde{g}_z|^2 / (\Delta_c^2 + \kappa^2) (1 + \kappa_{\text{nad}})$ and non-adiabatic corrections: $\kappa_{\text{nad}} = \kappa^2 / (\Delta_c^2 + \kappa^2) + \kappa^2 / \Delta_c^2$. The operators in the SCOL part are the total spin per site $\hat{\mathbf{S}}_i^2 = \sum_\nu \hat{S}_{\nu,i}^2$ and the particle number per site operator $\hat{n}_i = \sum_\sigma \hat{n}_{\sigma,i}$. The matter will self-organise in such a way that the cavity induced interaction term is maximised for $\Delta_c > 0$ (red detuned) and minimised for $\Delta_c < 0$ (blue detuned). In addition there will be competition between the typical local (short-range) processes in the Hubbard model ($\propto U$ and t_0), “local” spin interactions ($\propto V_C$) and the “global” (long-range) cavity induced spin interactions ($\propto V_Q$). Typical frequencies of the analogous system without the optical lattice are $\kappa \sim |\Delta_c| \sim \text{MHz}$ and recoil energy $E_R \sim \hbar \times 4\text{kHz}$ [3]. In the case of SCOL ($V_Q = 0$), the particular sign of the magnetic interaction V_C is fixed by the nature of the atom to be either Ferromagnetic (F) for $V_C < 0$ or Antiferromagnetic (AF) for $V_C > 0$. Typical atoms used are: ^{87}Rb (F), ^{7}Li (F) or ^{23}Na (AF) with fixed $V_C/U \sim (-0.005, -0.23, 0.04)$ [2]. In the system with the cavity induced interaction, in contrast to the SCOL ($V_Q = 0$), the parameters to trigger different magnetic behaviour can be tuned externally via the detuning Δ_c . We study configurations such that the pump incidence angle maximising diffraction generates homogenous coupling ($\varphi_{z,i} = 1$) or staggered density coupling in the diffraction minima ($\varphi_{z,i} = (-1)^i$) similar to the current experimental setting (with the pump at 90° with respect to the cavity axis). More elaborate scenarios occur depending on the pumps and the cavity setup [16, 25].

Magnetic interactions. In experiments, it is possible to prepare the system with flexibility regarding different spin components without the lattice [3]. We choose commensurate fillings in the lattice to study the behaviour between Mott-insulator (MI) phases driven by U and the magnetic dynamics. Under these conditions, the structure of the phase diagram with respect to the system without the cavity is well known [1, 2, 31]. Additionally, we consider the situations where there is an underlying linear (quadratic) magnetic field shift either favouring one of the spin components “ $\uparrow\downarrow$ ” (“0”) relevant for F (AF) ordering. The shift terms are: $\epsilon_{\uparrow\downarrow} \sum_i \hat{S}_{z,i}$ (linear shift) and $\epsilon_0 \sum_i \hat{n}_{0,i}$ (quadratic shift) [2], where ϵ_σ is an arbitrary small perturbation.

In the case where $V_C = 0$ the behaviour of the three components is simplified as the “0” component decouples

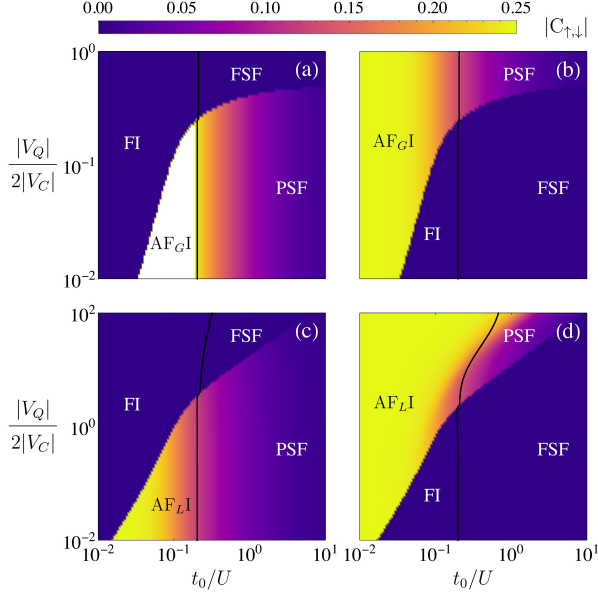


Figure 2. Phase diagrams of magnetic order competition scenarios. The spin correlations $|C_{\uparrow,\downarrow}|$ for different choices of ratios of cavity induced (global) V_Q and intrinsic (local) V_C magnetic interactions. The competition between interactions triggers QPT's between $AF_{G/L}I \leftrightarrow F$ as a function of the ratio between tunnelling t_0 and Hubbard repulsion U . Black lines correspond to the value of the approximated boundary between MI and SF states, where total on-site number fluctuations are half of the limit $t_0 \gg U$, $\max(\Delta(\hat{n}_i)^2) = (N_s - 1)/N_s$, there is not a clear critical point due to finite size effects and the dimensionality considered. Parameters are: (a) $V_C > 0$, $V_Q < 0$, $\varphi_{z,i} = 1$, (b) $V_C < 0$, $V_Q > 0$, $\varphi_{z,i} = 1$, (c) $V_C > 0$, $V_Q > 0$, $\varphi_{z,i} = (-1)^i$, (d) $V_C < 0$, $V_Q < 0$, $\varphi_{z,i} = (-1)^i$.

from the spin dynamics by the form of the interaction. A general state in this limit can be written as $|\Psi\rangle = |\Psi_0\rangle \otimes |\Psi_{\uparrow,\downarrow}\rangle$ [21].

Cavity induced ferromagnetic and polar configurations ($V_C = 0$). For $\varphi_{z,i} = 1$ and negative coupling $V_Q < 0$, the behaviour is intuitive as the system maximises the population of either one of the spin components “ $\uparrow\downarrow$ ” depending on the sign of $\epsilon_{\uparrow\downarrow} \neq 0$, $\epsilon_0 \geq 0$ having a ferromagnet. When $V_Q > 0$ if $\epsilon_{\uparrow\downarrow} = 0$ and $\epsilon_0 < 0$ then the “0” component gets maximised (Polar). Similarly, for $\varphi_{z,i} = (-1)^i$ when $V_Q > 0$, $\epsilon_0 < 0$, the system is always F with maximal “ $\uparrow\downarrow$ ” component depending on sign of $\epsilon_{\uparrow\downarrow}$. In all these cases, the system follows the dynamics of single either “ $\uparrow\downarrow$ ” or “0” component Bose-Hubbard model and the phase diagram is magnetically trivial, as the system ground state is fully polarised.

Cavity induced anti-ferromagnets ($V_C = 0$). Interestingly, if $V_Q > 0$, and $\epsilon_0 > 0$ for $\varphi_{z,i} = 1$, the situation is not magnetically trivial. Now AF order takes over because the “0” component gets minimised due to energetics and its dynamics are decoupled. The populations of atomic components “ \uparrow ” and “ \downarrow ” are the

same, but in order to minimise total population fluctuations for large U , the MI state exhibits large fluctuations in the “ $\uparrow\downarrow$ ” components. These large fluctuations in “ $\uparrow\downarrow$ ” components are a consequence of the minimisation of total atomic fluctuations as U opens the Mott gap. The component fluctuations are linked via the quantum correlations. In this limit, there is a simple relation, $\Delta(\hat{n}_i)^2 = 2C_{\uparrow,\downarrow} + 2\Delta(\hat{n}_{\uparrow\downarrow,i})^2$, with $\Delta(\hat{X})^2 = \langle \hat{X}^2 \rangle - \langle \hat{X} \rangle^2$, $C_{\uparrow,\downarrow} = \text{cov}(\hat{n}_{\uparrow,i}, \hat{n}_{\downarrow,i})$ and $\text{cov}(\hat{X}, \hat{Y}) = \langle \hat{X}\hat{Y} \rangle - \langle \hat{X} \rangle \langle \hat{Y} \rangle$. Deep in the MI, $\Delta(\hat{n}_i)^2 = 0$, $\Delta(\hat{n}_{\uparrow\downarrow,i})^2 = 1/4$ and $C_{\uparrow,\downarrow} = -1/4$. Moreover, the ground state is a massively degenerate insulator with “global” AF order, the degeneracy of the ground-state grows like $g_G \sim 2^{N_s-1/3}(N_s)^{-1/2}$. The atoms are anti-correlated, while fluctuations $\Delta(\hat{n}_{\uparrow\downarrow,i})^2$ are larger than the total number of particle per site quantum fluctuations. As U decreases approaching the MI-SF transition the spin correlations decrease. Deep in the SF state there are no spin correlations. In this limit, the systems becomes a paramagnet ($C_{\uparrow,\downarrow} \rightarrow 0$). Surprisingly for $V_Q < 0$ with $\varphi_{z,i} = (-1)^i$, we find that a “local” insulating AF state (degeneracy $g_L = 2$) with large correlations between the two components is the ground state for large U and a SF paramagnetic state is reached as $U \rightarrow 0$. In the $U \gg t_0$ the ground state has the following structure for the “global” AF (AF_G),

$$\dots | \dots \uparrow\downarrow\downarrow\uparrow \dots \rangle | \dots \uparrow\downarrow\downarrow\uparrow \dots \rangle | \dots \uparrow\downarrow\downarrow\uparrow \dots \rangle \\ | \dots \downarrow\uparrow\uparrow\downarrow \dots \rangle | \dots \downarrow\uparrow\uparrow\downarrow \dots \rangle | \dots \downarrow\uparrow\uparrow\downarrow \dots \rangle \dots$$

and for the “local” AF (AF_L),

$$| \dots \uparrow\downarrow\uparrow\downarrow \dots \rangle | \dots \downarrow\uparrow\uparrow\downarrow \dots \rangle, \dots$$

with $|\uparrow\rangle = |0,1\rangle$ and $|\downarrow\rangle = |1,0\rangle$ in the Fock space representation $|n_{i,\downarrow}, n_{i,\uparrow}\rangle$. The fact that the $\uparrow\downarrow$ components are anti-correlated for large U in all configurations, implies that the many-body insulating AF state cannot be represented as a product state in each component: $|\Psi_{\uparrow,\downarrow}\rangle \neq |\Psi_{\uparrow}\rangle \otimes |\Psi_{\downarrow}\rangle$. These facts are independent of dimensionality. Thus, the components are entangled and the system has a natural bipartite structure to analyse with its spin components. The emergence of SF order is correlated with the suppression of spin correlations, as it favours a paramagnetic state.

Competition of Magnetic Order. Simplifying our analysis, we choose the case where the “0” component is empty, experimentally achievable [3]. In addition to U , the atoms experience local and long range magnetic interactions. Therefore, these three mechanisms can compete. Interestingly, even if V_Q is fixed by nature for a given alkali atom, modifying the pump angle allows to investigate the AF and F order competition. The emergent phases of quantum matter can be understood by analysing the behaviour of the number fluctuations for “ $\uparrow\downarrow$ ” components and the total number fluctuations extracting the quantum correlations ($C_{\uparrow,\downarrow}$). This information might be accessed experimentally via in situ measurements[3] or

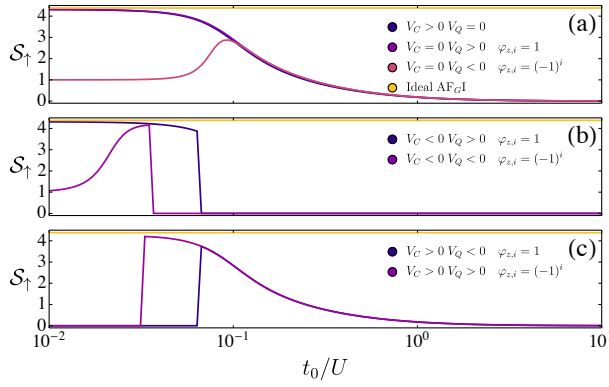


Figure 3. **Entanglement entropy of spin components for magnetic order competition scenarios.** The entanglement entropy S_{\uparrow} with parameter values: $|V_Q|/|V_C| = 0.05$, $V_C = 0.03U$. S_{\uparrow} reflects the degeneracy in the ground state configurations and the local or global nature of AF order of insulating states.

direct measurements of AF correlations[32, 33] similar to fermionic systems. We perform exact diagonalization simulations and construct the ground state phase diagrams in Fig. 2 (a-d). Intuitively, the competition between F and AF order in the homogenous case occurs by choosing different signs in the effective couplings $V_{Q/C}$. Counterintuitively, pumping at 90° , the competition scenario occurs for the same sign of coupling strengths $V_{Q/C}$. The ratio V_Q/V_C determines the passage starting from insulating (I) AFI (FI) to remain AFI (FI) or having a 1st order transition to a FI (AFI) state depending on strength of the on-site repulsion in the limit $U \gg t_0$, while reaching SF of Paramagnetic (PSF) or Ferromagnetic character (FSF) for $U \ll t_0$. As a function of the lattice depth (effectively t_0/U) one can have for a fixed ratio V_Q/V_C the following scenarios for competition possibilities for both pump angle setups,

$$FI \leftrightarrow AFI \leftrightarrow PSF \quad \text{or} \quad AFI \leftrightarrow FI \leftrightarrow FSF$$

In general, via the cavity induced magnetic interactions it is possible to control whichever scenario one would desire.

Spin Entanglement. Typically entanglement partitioning considers spatial subsystems. However, we are interested in how the entanglement between spins projections behaves across the whole system in the $AFM \leftrightarrow PSF$ region of the phase diagram. Here the quantum correlations range between $-1/4$ and 0 . To do this, we trace over different different spin projection subsystems. Then the reduced density matrix for the spin components $\sigma = \uparrow\downarrow$ is given by,

$$\rho_{\sigma} = \text{Tr}_{\neq\sigma}[\rho] = \text{Tr}_{-\sigma}[\text{Tr}_0[\rho]] \quad (3)$$

where $\text{Tr}_{\sigma}[\cdot]$ is the partial trace with respect to the atomic states with projection σ over all the lattice sites for $\sigma \in \{\downarrow, 0, \uparrow\}$. We analyse the entanglement in the system components by computing the entanglement entropy $S_{\sigma} = -\text{Tr}[\rho_{\sigma} \log_2 \rho_{\sigma}]$.

We find that S_{σ} gets maximised in the insulator region of the phase diagram in both the SCOL ($V_C > 0, V_Q = 0$) and the SQOL ($V_C = 0, V_Q > 0$) homogenous coupling with maximum value, $\max(S_{\sigma}) = \log_2(g_G)$. This is the entanglement entropy of the ideal AFI in the $t_0 \ll U$ limit. This is expected, as $|C_{\uparrow,\downarrow}|$ becomes maximal in the atomic limit. Surprisingly, this is not the case for the SQOL and pumping at 90° . The difference can be traced back to the degeneracy in the ground state in the limit $t_0 \ll U$ for 90° . The ideal AFI is just double degenerate leading to $S_{\sigma} = 1$. We find non monotonic character in the 90° setup in S_{σ} . This behaviour arises because the degeneracy increases as the MI-SF transition is reached and the system becomes gapless. S_{σ} increases reaching a maximum value, which later vanishes towards the PSF state, see Fig. 3 (a). Interestingly, when competition between F and AF occurs the entanglement entropy shows the 1st order character of the QPT, with its characteristic jump. In the AF-F transition, as expected for a single component system being completely polarised, S_{σ} gets totally suppressed. The behaviour of S_{σ} in the Fig.3(b) and 3(c) shows the impact of competition and degeneracy in the ground state as the 1st order transition occurs for lower values of t_0/U in the case of 90° pumping with respect to homogenous pumping. Depending on the critical value for the transition to the F state, it is possible to see the branch of either global or local AFI state in the signal of S_{σ} while the AF correlations hide this characteristic entirely, see Fig. 3(b). Therefore, one can conclude that AFI's have more resilient spin entanglement. This regime can be accessed at lower lattice depths and should be useful for quantum information purposes. This robustness could be exploited in large realisations of gates, similar to what has been achieved in classical optical lattices in the MI limit regarding two q-bit gates with thousands of atoms [34].

Spinor quantum optical lattices offer great flexibility to investigate the nature of different magnetic quantum phases of matter. In the simplest setup, global/local anti-ferromagnets can be investigated. Moreover, the system properties can be externally tuned independent of the particular nature of atomic species by properly choosing the geometry of light. In a single setup it is possible to investigate several scenarios regarding competition. Moreover, the system naturally supports by the light-induced non-magnetic interaction terms where density wave order and other exotic phases emerge (multi-mode,bonds) [23, 25]. Other finite range interactions are possible with rare-earth atoms [35], where competition finite range density dependent terms and can be combined. Additional advances with rare-earth fermions [36] and inclusion of cavity interplay should extend the picture of Kondo physics. Using geometrically frustrated anti-ferromagnets by modifying the COL [37, 38] will generate complex phases of quantum matter with emergent degrees of freedom and possibly modified quantum spin

liquids [39, 40]. It should be feasible to consider the interplay with static gauge fields [41, 42] and cavity generated spin-orbit coupling via Raman transitions [43]. Moreover, a plethora of possibilities using dynamical gauge fields can be considered [44, 45]. These can be useful for quantum simulations of high energy physics beyond local models.

From the quantum information perspective, the fact that entanglement can be tailored on demand and is robust between spin components globally, should allow to control the formation of structures for their manipulation and encoding. These useful features can be further explored relative to quantum information and topological order [46]. In combination with measurement it is feasible to have dynamical order control in passive measurement setups [27, 28], the inclusion of feedback protocols to tailor criticality, their dynamics and study the interplay with time crystals [47–51].

We thank R. Jauregui and I. B. Mekhov for useful discussions. This work was supported by the grants UNAM, DGAPA-PAPIIT: IN109619 and CONACYT Ciencia Básica: A1-S-30934. K. L.-M. thanks DGAPA-UNAM PAPIIT program for financial support. A. H. C. acknowledges financial support from CONACYT. We acknowledge infrastructure support for the computations from the “Laboratorio de Simulaciones Computacionales para Sistemas Cuánticos” in LANMAC (LSCSC-LANMAC) at IF-UNAM.

Electrodynamical Toolbox for Quantum Magnetism. *Phys. Rev. Lett.* **122**, 113603 (2019).

- [11] B. Buča, and D. Jaksch, Dissipation Induced Nonstationarity in a Quantum Gas. *Phys. Rev. Lett.* **123**, 260401 (2019).
- [12] E. I. Rodríguez Chiacchio, and A. Nunnenkamp, Dissipation-Induced Instabilities of a Spinor Bose-Einstein Condensate Inside an Optical Cavity. *Phys. Rev. Lett.* **122**, 193605 (2019).
- [13] Z Li, et. al. Nonlinear Floquet dynamics of spinor condensates in an optical cavity: Cavity-amplified parametric resonance, *Phys. Rev A* **100**, 033617 (2019).
- [14] R. Landig, et. al. Quantum phases from competing short- and long-range interactions in an optical lattice. *Nature* **532**, 476 (2015).
- [15] P. Zupancic, et. al. P-Band Induced Self-Organization and Dynamics with Repulsively Driven Ultracold Atoms in an Optical Cavity. *Phys. Rev. Lett.* **123**, 233601 (2019).
- [16] S. F. Caballero-Benitez, and I. B. Mekhov, Quantum optical lattices for emergent many-body phases of ultracold atoms. *Phys. Rev. Lett.* **115**, 243604 (2015).
- [17] N. Dogra, F. Brennecke, S. D. Huber and T. Donner, Phase transitions in a Bose-Hubbard model with cavity-mediated global-range interactions, *Phys. Rev. A* **94**, 023632 (2016).
- [18] L. Himbert, et. al. Mean-field phase diagram of the extended Bose-Hubbard model of many-body cavity quantum electrodynamics. *Phys. Rev. A* **99**, 043633 (2019).
- [19] R. Lin, L. Papariello, P. Molignini, R. Chitra, and A. U. J. Lode, Superfluid-Mott-insulator transition of ultracold superradiant bosons in a cavity, *Phys. Rev. A* **100**, 013611 (2019).
- [20] C. M. Halati, A. Sheikhan, H. Ritsch, and C. Kollat, Numerically Exact Treatment of Many-Body Self-Organization in a Cavity. *Phys. Rev. Lett.* **125**, 093604 (2020).
- [21] See supplemental material.
- [22] W. Kozlowski, S. F. Caballero-Benitez, and I. B. Mekhov, Probing Matter-Field and Atom-Number Correlations in Optical Lattices by Global Nondestructive Addressing. *Phys. Rev. A* **92**, 013613 (2015).
- [23] S. F. Caballero-Benitez, and I. B. Mekhov, Bond order via light-induced synthetic many-body interactions of ultracold atoms in optical lattices. *New J. Phys.* **18**, 113010 (2016).
- [24] C. Maschler, I. B. Mekhov, and H. Ritsch, Ultracold atoms in optical lattices generated by quantized light fields. *Eur. Phys. J. D* **46**, 545-560 (2008).
- [25] S. F. Caballero-Benitez, G. Mazzucchi, and I. B. Mekhov, Quantum simulators based on the global collective light-matter interaction. *Phys. Rev. A* **93**, 063632 (2016).
- [26] A. Camacho-Guardian, R. Paredes, and S. F. Caballero-Benitez, Quantum Simulation of Competing Orders with Fermions in Quantum Optical Lattices. *Phys. Rev. A* **96**, 051602(R)(2017)
- [27] G. Mazzucchi, W. Kozlowski, S. F. Caballero-Benitez, T. J. Elliott, and I. B. Mekhov, Quantum Measurement-induced Dynamics of Many-Body Ultracold Bosonic and Fermionic Systems in Optical Lattices. *Phys. Rev. A* **93**, 023632 (2016).
- [28] G. Mazzucchi, S. F. Caballero-Benitez, and I. B. Mekhov, Quantum measurement-induced antiferromagnetic order and density modulations in ultracold Fermi gases in optical lattices . *Sci. Rep.* **6**, 31196 (2016).

* scaballero@fisica.unam.mx

- [1] M. Lewenstein, A. Sanpera, and V. Ahufinger. *Ultracold atoms in optical lattices: Simulating Quantum Many-Body Systems*. Oxford University Press (2012).
- [2] P. T. Brown, et. al. Spin-imbalance in a 2D Fermi-Hubbard system. *Science* **357**, 1385 (2017).
- [3] C. S. Chiu, G. Ji, A. Mazurenko, D. Greif and M. Greiner, Quantum State Engineering of a Hubbard System with Ultracold Fermions. *Phys. Rev. Lett.* **120**, 243201 (2018).
- [4] G. Salomon, et. al. Direct observation of incommensurate magnetism in Hubbard chains. *Nature* **565**, 56 (2019).
- [5] F. Görg, et. al. Enhancement and sign change of magnetic correlations in a driven quantum many-body system. *Nature* **553**, 481 (2018).
- [6] M. Landini, et. al. Formation of a Spin Texture in a Quantum Gas Coupled to a Cavity, *Phys. Rev. Lett.* **1** **20**, 223602 (2018).
- [7] N. Dogra, et. al. Dissipation-induced structural instability and chiral dynamics in a quantum gas. *Science* **366**, 1496 (2019).
- [8] R. M. Kroese, Y. Guo, V. D. Vaidya, J. Keeling, and B. L. Lev, Spinor Self-Ordering of a Quantum Gas in a Cavity. *Phys. Rev. Lett.* **121**, 163601 (2018).
- [9] J. A. Muniz, et. al. Exploring dynamical phase transitions with cold atoms in an optical cavity. *Nature* **580**, 602 (2020).
- [10] F. Mivehvar, H. Ritsch, and F. Piazza, Cavity-Quantum-

[29] S. F. Caballero-Benitez, and I. B. Mekhov, Quantum properties of light scattered from structured many-body phases of ultracold atoms in quantum optical lattices. *New J. Phys.* **17** 123023 (2015).

[30] D. M. Stamper-Kurn, and M. Ueda, Spinor Bose gases: Symmetries, magnetism, and quantum dynamics, *Rev. Mod. Phys.* **85**, 1191 (2013).

[31] L. de Forges de Parny, and V. G. Rousseau, Phase diagrams of antiferromagnetic spin-1 bosons on a square optical lattice with the quadratic Zeeman effect. *Phys. Rev. A* **97**, 023628 (2018).

[32] T. A. Hilker, et. al., Revealing Hidden Antiferromagnetic Correlations in Doped Hubbard Chains via String Correlators. *Science* **357**, 484 (2017).

[33] R. A. Hart, et. al. Observation of antiferromagnetic correlations in the Hubbard model with ultracold atoms. *Nature* **519**, 211 (2015).

[34] B. Yang, et. al. Cooling and entangling ultracold atoms in optical lattices. *Science* **369**, 550 (2020).

[35] S. Baier, et. al. Extended Bose-Hubbard Models with Ultracold Magnetic Atoms. *Science* **352**, 201 (2016).

[36] L. Rieger, et. al. Localized Magnetic Moments with Tunable Spin Exchange in a Gas of Ultracold Fermions. *Phys. Rev. Lett.* **120**, 143601 (2018).

[37] L. Santos, et. al. Atomic Quantum Gases in Kagome Lattices. *Phys. Rev. Lett.* **93**, 030601 (2004).

[38] T.-H. Leung, et. al. Interaction-Enhanced Group Velocity of Bosons in the Flat Band of an Optical Kagome Lattice, *Phys. Rev. Lett.* **125**, 133001 (2020).

[39] L. Balents, Spin liquids in frustrated magnets. *Nature* **464**, 199 (2010).

[40] C. Broholm, et. al. Quantum spin liquids. *Science* **367**, 263 (2020).

[41] G. Jotzu, et. al. Experimental realization of the topological Haldane model with ultracold fermions. *Nature* **515**, 237 (2014).

[42] M. Aidelsburger, et. al. Realization of the Hofstadter Hamiltonian with Ultracold Atoms in Optical Lattices.

[43] R. M. Kroese, Y. Guo, and B. L. Lev, Dynamical Spin-Orbit Coupling of a Quantum Gas. *Phys. Rev. Lett.* **123**, 160404 (2019).

[44] N. Goldman, G. Juzeliūnas, P. Ohberg, and I. B. Spielman, Light-induced gauge fields for ultracold atoms. *Rep. Prog. Phys.* **77** 126401 (2014)

[45] L. Barbiero, et. al., Coupling ultracold matter to dynamical gauge fields in optical lattices: From flux attachment to \mathbb{Z}_2 lattice gauge theories. *Sci. Adv.* **5**, eaav7444 (2019).

[46] B. Zeng, X. Chen, D.-L. Zhou, and X. G. Wen *Quantum Information Meets Quantum Matter-From Quantum Entanglement to Topological Phase in Many-Body Systems*, Springer, New York, NY (2019).

[47] D. A. Ivanov, T. Yu. Ivanova, S. F. Caballero-Benitez, and I. B. Mekhov, Feedback-Induced Quantum Phase Transitions Using Weak Measurements. *Phys. Rev. Lett.* **124**, 010603 (2020).

[48] D. A. Ivanov, T. Yu. Ivanova, S. F. Caballero-Benitez, and I. B. Mekhov, Cavityless self-organization of ultracold atoms due to the feedback-induced phase transition. *Sci. Rep.* **10**, 10550 (2020).

[49] G. Mazzucchi, S. F. Caballero-Benitez, D. A. Ivanov and I. B. Mekhov, Quantum optical feedback control for creating strong correlations in many-body systems. *Optica* **3**, 1213 (2016).

[50] Y. Fuji and Y. Ashida, Measurement-induced quantum criticality under continuous monitoring. *Phys. Rev. B* **102**, 054302 (2020).

[51] K. Kroeger, et. al., Continuous feedback on a quantum gas coupled to an optical cavity. *New J. Phys.* **22**, 033020 (2020).

SUPPLEMENTAL MATERIAL: SPIN ENTANGLEMENT AND ORDER COMPETITION VIA LONG-RANGE INTERACTIONS IN SPINOR QUANTUM OPTICAL LATTICES

Classical optical lattice model with spin $F = 1$. The Bose-Hubbard Hamiltonian [1] with spin [2] (Spinor Bose-Hubbard Model) is $\mathcal{H}_{\text{SCOL}} = \mathcal{H}_U + \mathcal{H}_C^S$, with

$$\begin{aligned} \mathcal{H}_U &= -t_0 \sum_{\sigma, \langle i, j \rangle} (\hat{b}_{i,\sigma}^\dagger \hat{b}_{j,\sigma} + \text{H.c.}) + \frac{U}{2} \sum_i \hat{n}_i (\hat{n}_i - 1) \\ \mathcal{H}_C^S &= \frac{V_C}{2} \sum_i \left(\hat{\mathbf{S}}_i^2 - 2\hat{n}_i \right) \end{aligned} \quad (4)$$

where $\langle i, j \rangle$ nearest neighbour pairs, $\hat{b}_{i,\sigma}^\dagger$ ($\hat{b}_{\sigma,i}$) are creation (annihilation) operators of bosonic atoms in site i , spin projections $\sigma \in \{\downarrow, 0, \uparrow\}$. The atom number operators are $\hat{n}_i = \sum_{\sigma} \hat{b}_{i,\sigma}^\dagger \hat{b}_{i,\sigma}$. The \mathcal{H}_C^S is the local spin interaction with coupling strength V_C and $\hat{\mathbf{S}}_i^2 = \hat{S}_{x,i}^2 + \hat{S}_{y,i}^2 + \hat{S}_{z,i}^2$. The tunneling amplitude of the bosons is t_0 , the on-site interaction is U . The effective parameters linked to the cavity can be calculated using Wannier functions,

$$t_0 = \int w(\mathbf{x} - \mathbf{x}_i) \left(\frac{\hbar^2}{2m} \nabla^2 - V_{\text{OL}}(\mathbf{x}) \right) w(\mathbf{x} - \mathbf{x}_j) d^{n_d} x, \quad (5)$$

$w(\mathbf{x})$ are the Wannier functions with i, j nearest neighbours. The classical optical lattice potential is $V_{\text{OL}}(\mathbf{x}) = V_0 \sum_{k=1}^{n_d} \sin^2(2\pi x_k/\lambda)$ with n_d the dimension. Typically, for a deep lattice $V_0 \gtrsim 10E_R$, then $t_0 \sim 0.1E_R$. where E_R is the recoil energy. The light-matter coupling coefficients in the direction $\nu \in x, y, z$ are,

$$J_\nu \varphi_{\nu,i} = \int |w(\mathbf{x} - \mathbf{x}_i)|^2 u_{V,\nu,c}^*(\mathbf{x}) u_{V,\nu,p}(\mathbf{x}) d^{n_d} x, \quad (6)$$

where $u_{V,\nu,c/p}$ are the effective cavity/pump mode functions from the vectorial contributions of the polarisation (see supplemental of [3]). For the cases considered here, the effective mode functions are such that the projections in the “ x ” and “ y ” direction are neglected due to energetics.

Many-body Quantum States.

The general many-body quantum state of the matter can be written as: $|\Psi\rangle = \sum_{\mathbf{k}} c_{\mathbf{k}} |\Psi_{\downarrow}\rangle_{k_{\downarrow}} \otimes |\Psi_0\rangle_{k_0} \otimes |\Psi_{\uparrow}\rangle_{k_{\uparrow}}$ with $|\Psi_{\sigma}\rangle_{k_{\sigma}} = |n_{\sigma,1}\rangle \otimes \dots \otimes |n_{\sigma,N_s}\rangle_{k_{\sigma}}$, where $\mathbf{k} = \{k_{\downarrow}, k_0, k_{\uparrow}\}$ denotes an element of the Hilbert space basis with amplitude $c_{\mathbf{k}}$. A particular combination of quantum

numbers for each spin component σ is k_σ . In the case where the “0” of the components is separable, we have: $c_{\mathbf{k}} = c_{k_0} c_{k_\downarrow, k_\uparrow} = c_{k_0} c_{\tilde{\mathbf{k}}}$ with $\tilde{\mathbf{k}} = \{k_\downarrow, k_\uparrow\}$. The state is: $|\Psi\rangle = |\Psi_0\rangle \otimes |\Psi_{\downarrow, \uparrow}\rangle$, with $|\Psi_0\rangle = \sum_{k_0} c_{k_0} |\Psi_0\rangle_{k_0}$ and $|\Psi_{\downarrow, \uparrow}\rangle = \sum_{\tilde{\mathbf{k}}} c_{\tilde{\mathbf{k}}} |\Psi_{\downarrow}\rangle_{k_\downarrow} \otimes |\Psi_{\uparrow}\rangle_{k_\uparrow}$. A completely separable state in the magnetic component sense (deep in the SF) is: $|\Psi\rangle = |\Psi_0\rangle \otimes |\Psi_\downarrow\rangle \otimes |\Psi_\uparrow\rangle$, with $|\Psi_\sigma\rangle = \sum_{k_\sigma} c_{k_\sigma} |\Psi_\sigma\rangle_{k_\sigma}$, then spin components are not correlated between each other.

Numerical methods.

Exact diagonalization simulations are performed with the effective Hamiltonian, equation (2). We use an optimised Lanczos scheme with sparse representation to find the ground states and the observables. As the Hilbert space grows geometrically, we are limited to small sizes. We consider lattices sizes of 6 (2x3), 8 (2x4) and 9 (3x3)

sites with three (effective 18 and 24 sites) and also effectively two (effective 12, 16, 18 sites) spin components with periodic boundary conditions. The Hilbert space sizes range from $\sim 10^6$ to $\sim 10^7$ basis states. Linear and quadratic magnetic shifts are $\epsilon_\sigma = \pm 10^{-8}U$.

* scaballero@fisica.unam.mx

- [1] M. Lewenstein, A. Sanpera, and V. Ahufinger. *Ultracold atoms in optical lattices: Simulating Quantum Many-Body Systems*. Oxford University Press (2012).
- [2] D. M. Stamper-Kurn, and M. Ueda, Spinor Bose gases: Symmetries, magnetism, and quantum dynamics, *Rev. Mod. Phys.* **85**, 1191 (2013).
- [3] M. Landini, et. al. Formation of a Spin Texture in a Quantum Gas Coupled to a Cavity, *Phys. Rev. Lett.* **120**, 223602 (2018).